Evolution of the electronic transport properties of V_6O_{11} and V_7O_{13} under pressure

S. K. Kim,[1,2] E. Colombier,[1,*] N. Ni,[1,2,†] S. L. Bud'ko,[1,2] and P. C. Canfield[1,2]
[1]*Ames Laboratory, Iowa State University, Ames, Iowa 50011, USA*
[2]*Department of Physics and Astronomy, Iowa State University, Ames, Iowa 50011, USA*
(Received 17 December 2012; revised manuscript received 14 March 2013; published 27 March 2013)

V_6O_{11} and V_7O_{13} are two members of the V_nO_{2n-1} Magnéli series ($n = 3$–9). At ambient pressure, V_6O_{11} manifests a metal to insulator (MI) transition near $T_{MI} = 170$ K and V_7O_{13} (the exception in the series that does not become insulating at ambient pressure) manifests an antiferromagnetic (AFM) transition with spin density wave character at $T_N = 43$ K. Temperature-dependent resistivity data for V_6O_{11} and V_7O_{13} were measured under pressures up to 7.52 and 6.40 GPa, respectively with critical pressures of $P_c^{MI} = 3.8$ GPa for V_6O_{11} and $P_c^{AFM} = 3.5$ GPa for V_7O_{13}. As the MI transition for V_6O_{11} is suppressed no features associated with an AFM transition in the resistivity are seen. Near the critical pressure for V_6O_{11} where the first-order MI transition disappears, a T^2 dependence of the low-temperature resistance can be found. On the other hand, in V_7O_{13} as the second-order, antiferromagnetic transition is brought towards $T = 0$, the resistivity shows a vanishing low-temperature region of Fermi-liquid-like behavior, consistent with proximity to a quantum critical point. Improved hydrostaticity of the pressurized sample space enhances the divergence of the T^2 coefficient for V_7O_{13} near the AFM critical pressure, 3.5 GPa.

DOI: 10.1103/PhysRevB.87.115140 PACS number(s): 62.50.−p, 72.15.Eb, 72.80.Ga, 74.40.Kb

I. INTRODUCTION

The metal to insulator (MI) transition has fascinated scientists for decades, and has, over the years, led to a great number of studies on materials that manifest this transition.[1] Of these materials, V_2O_3 and VO_2 are classic examples with the former considered the prototypical Mott-Hubbard insulator. In these and other systems with MI transitions, pressure is used to tune the system, often suppressing T_{MI}. For V_2O_3, with an ambient pressure T_{MI}= 176 K on warming, applied pressure causes a decrease in T_{MI}, with it being fully suppressed by 2.6 GPa.[2] For $P \geqslant 2.6$ GPa, quadratic behavior is seen in the low-temperature resistivity. On the other hand, VO_2 has a MI transition at T_{MI}= 340 K and no magnetic ordering was observed down to low temperatures.[1,3,4] With applied pressure, the T_{MI} was seen to increase linearly at 0.82 K/GPa.[5]

Modifying the structure is another method of tuning a system. The homologous V_nO_{2n-1} ($n = 3$–9) Magnéli series spans the compositional and structural range between VO_2 and V_2O_3 with n units of VO_2 (rutile) separated by a V_2O_3-like face-sharing shear plane. T_{MI} is found for $n = 3$–6, 8, and 9 with $n = 7$ having $T_{MI} = 0$ and instead showing features consistent with spin density wavelike antiferromagnetic order with a transition temperature (T_N) at 45 K.[4,6–11] Combining the structural and pressure tuning, the effect of pressure on several of the Magnéli series compounds have already been studied.[11–17] Systematic studies by Canfield *et al.*[11,13,14] measured the transport properties of V_nO_{2n-1} ($n = 4$–8) for pressures $P < 2$ GPa. T_{MI} was found to decrease with pressure to varying degrees for $n = 4, 5, 6$, and 8. For V_7O_{13} the T_N also decreased with increasing pressure at a rate of −7.5 K/GPa.[11] Particularly interesting was V_8O_{15} where T_{MI} could be fully suppressed by these modest pressures, revealing the same resistive antiferromagnetic (AFM) signature that was seen in V_7O_{13}. This discovery suggested that the spin density wavelike order in V_7O_{13} was not anomalous, but was in fact a general feature of the V_nO_{2n-1} system.

Pressure studies of V_7O_{13} that were initially performed up to 2 GPa[11,13,14] and later extended up to 3.5 GPa[15] have shown that the AFM transition temperature steadily decreases with applied pressure until, near 3.4 GPa, it disappears in measurements down to 1.7 K. Near this critical pressure (P_c^{AFM}), Ueda *et al.*[15] found a $T^{3/2}$ dependence for resistivity at base temperatures, indicating non-Fermi-liquid behavior near a quantum critical point (QCP). V_8O_{15}, also measured under pressure up to 3.5 GPa, showed a suppression of its MI transition with pressure until at 1.34 GPa, where the MI transition disappeared and revealed a feature associated with AFM ordering. Further increase of pressure suppressed this feature until at $P_c^{AFM} = 3.4$ GPa, where it is driven to $T = 0$. For V_8O_{15}, continued T^2 dependence was seen at low temperatures near the AFM critical pressure.[15]

In order to further study the effects of pressure on the V_nO_{2n-1} series, in this work we present high-pressure ($P < 8$ GPa) measurements of the electrical resistivity of V_6O_{11} and V_7O_{13} for $0.3 < T < 300$ K. For V_6O_{11} we find that the MI transition can be suppressed to zero by $P \approx 3.8$ GPa and that the behavior of $\rho(T,P)$ is consistent with the suppression of a first-order phase transition to zero rather than a second-order one. As T_{MI} is suppressed, though, no features associated with AFM ordering were seen to emerge. For V_7O_{13}, the spin density wavelike transition can be suppressed to zero by $P_c^{AFM} \sim 3.5$ GPa and the behavior of ρ is consistent with a second-order transition being driven to zero, with the coefficient A, of $\rho \propto AT^2$, diverging at P_c^{AFM}. Finally we can create a composite phase diagram for V_6O_{11}, V_7O_{13}, and V_8O_{15} that provides some rationalization for why V_6O_{11} does not manifest the SDW-like state seen in V_7O_{13} and V_8O_{15}.

II. EXPERIMENTAL METHODS

The V_6O_{11} and V_7O_{13} single crystals were prepared in a two-step process. First, stoichiometric mixtures of powdered

V_2O_3 and VO_2 were reacted to form polycrystalline V_6O_{11} or V_7O_{13}. Then the polycrystalline material was ground and mixed with a few tens of mg of $TeCl_4$ and sealed in an evacuated quartz tube. The tube was placed horizontally in a thermal gradient furnace where the end of the tube with starting material is kept near 1050 °C and the other side set to be near 950 °C. Several weeks were needed to grow the single crystals.[14,18]

Given the subtle differences in the powder x-ray diffraction spectra of the large unit cells of triclinic V_6O_{11} and V_7O_{13}, and given the distinct ordering temperatures and phase transitions of the various V_nO_{2n-1} members,[6,11,14,19,20] temperature-dependent resistance and magnetization were used to confirm the characteristic features of the V_6O_{11} and V_7O_{13} samples. These measurements were conducted in a Quantum Design Physical Properties Measurement System (PPMS) and a Magnetic Properties Measurement System (MPMS) respectively.

For resistivity measurements under pressure rectangular rods with linear dimensions of approximately 700 × 150 × 50 μm^3 were used. The rods were formed by polishing the larger crystal into shape with 2400 grit sandpaper. There were no efforts to have the faces of the rectangular rods oriented along any of the triclinic crystallographic directions. Four 12.5-μm diameter gold wires were attached using DuPont 4929N silver paint in a linear four wire arrangement. Due to the small dimensions of the sample, errors of up to 30% in absolute resistivity values are expected.

A modified Bridgman cell[21] was used for all pressure measurements with a 1:1 mixture of Fluorinert 70 and Fluorinert 770 (FC70 : FC770) or a 1:1 mixture of n-pentane and iso-pentane serving as the liquid pressure medium. The hydrostatic limit of a pressure transmitting medium is the pressure at which the liquid medium begins to solidify at ∼300 K (room temperature). Given that the increase of pressure is typically done at room temperature, a higher degree of hydrostaticity is expected for pressures less than the hydrostatic limit. Above the hydrostatic limit, minute pressure gradients due to the crystalline or glassy pressure transmitting media can occur. For 1:1 FC70:FC77 and 1:1 n-pentane : iso-pentane, the hydrostatic limits are ∼1 and 6.5 GPa, respectively.[22–24] (The pressure-dependent properties of Fluorinert 770 are expected to be the same as that of Fluorinert 77.) More hydrostatic conditions are expected for the 1:1 n-pentane : iso-pentane mixture. The 1:1 FC70 : FC770 mixture was used for all V_6O_{11} and several V_7O_{13} measurements under pressure. For V_7O_{13}, the 1:1 n-pentane : iso-pentane mixture was also used to see if the degree of hydrostaticity of the medium had measurable effects.

These Bridgman cells were designed to work in conjunction with a PPMS. Measurements for $2 \leqslant T \leqslant 6$ K were taken with a warming rate of 0.1 K/min and for $6 \leqslant T \leqslant 30$ K a warming rate of 0.2 K/min was used. At the sample space, a temperature lag of at most 100 mK is expected for these warming rates.[25] Low-temperature measurements down to 0.47 and 0.32 K were conducted on V_6O_{11} and V_7O_{13} respectively, using a CRYO Industries of America ^{3}He system. Unless otherwise noted, only warming data are shown in the figures.

The pressure within the sample space was determined by the superconducting temperature of a lead sample that was also included in the sample space. Measurements of this transition were done by stabilizing at each temperature before collecting data to further minimize any temperature lag. The pressure difference in the sample space between room temperature and at 30 K is less than 0.1 GPa.[25] The superconducting transition width of the lead samples gives an estimate of the level of hydrostaticity. For measurements with the 1:1 n-pentane : iso-pentane mixture, the Pb SC transition width is typically 15 mK[26] which at 3.5 GPa corresponds to a pressure gradient of 0.04 GPa. Measurements with the 1:1 FC70 : FC770 liquid media usually show a transition width of 40 mK,[26] which indicates a gradient of 0.12 GPa at 3.5 GPa.

When measuring V_6O_{11}, the ambient pressure structural transition at 170 K often destroyed the samples, making them unusable for further measurements. This is most likely caused by the strains associated with changing V-V bond lengths as the MI transition occurs. Of the V_nO_{2n-1} family, V_6O_{11} exhibits the largest such change with a V-V bond length expanding by ∼0.5 Å on cooling through T_{MI}.[14] Fortuitously, even a small amount of hydrostatic pressure seems to prevent the sample from irreversibly cracking during the structural transition, allowing for measurements under pressure.[14] In order to work around this structural degradation at ambient pressure, a V_6O_{11} crystal was polished into a long rectangular rod and separated into several pieces, one of which was used for these preliminary resistance measurements. As a result of this, for V_6O_{11}, the ambient pressure resistivity curve could not be measured beforehand for all sets of pressure measurements (each set denoted as cell 1, 2, and so on). However, for cell 1 after several pressure measurements, the V_6O_{11} sample survived the depressurization process and was then used to measure the ambient pressure, temperature-dependent resistivity. This provides the only full temperature range measurement of V_6O_{11} at ambient pressure that could be compared to higher pressure measurements. V_6O_{11} samples from all other pressure measurements were lost when the sample space was depressurized. For $P \gtrsim 3$ GPa, the suppression rate of the ambient temperature resistivity values with respect to pressure were fairly consistent, at close to -6×10^{-6} Ω cm GPa^{-1}. Therefore, all V_6O_{11} measurements were normalized to cell 1. This was done by having the ambient temperature resistivity of the initial pressure measurement of each cell normalized to a linear interpolation of the same value from the pressure measurements of cell 1. For the few $P < 3$ GPa measurements, these curves were also normalized to cell 1 in a similar manner, except the rate of suppression of the resistivity value for cell 1 was only defined by two points, one at ambient pressure and one at 3.52 GPa.

For resistivity measurements of V_6O_{11} at $P = 0.84$ and 1.64 GPa, at least one of the contacts on the sample was electrically connected to the pressure cell itself. This likely contributed to the measured negative slope of $\rho(T)$ of the sample for these two pressures. However, at these low pressures, only T_{MI} was determined from these data.

V_7O_{13} remains metallic and avoids the structural phase transition associated with the MI transitions found for the rest of the series, thus allowing for ambient pressure resistivity measurements for all samples. A comparison of the R/R(300 K) for all the samples at ambient pressure shows the curves very nearly lying on top of each other. Therefore, all sets of V_7O_{13} measurements were normalized to that of one

set by having the ambient pressure and temperature resistivity of each cell multiplicatively normalized to that of one cell and this normalization factor was propagated to the resistivity measurements under pressure.

III. RESULTS

A. V_6O_{11}

The ambient pressure, temperature-dependent resistivity for V_6O_{11} can be seen in Fig. 1(a) for cooling and warming. This measurement was taken using a sample that was retrieved after being measured under several pressures up to 5.44 GPa. A comparison of cooling and warming data shows the hysteresis [inset of Fig. 1(a)] of the first-order MI transition near 170 K. Erratic jumps in the resistivity at low temperatures are attributed to cracks in the sample due to the structural transition that accompanies the MI transition. The hysteretic behavior of the MI transition exists for all resistivity measurements for $0 \leqslant P \leqslant 3.52$ GPa. For clarity, only warming data for selected resistivity curves from four sets of pressure cell measurements are shown for V_6O_{11} in Figs. 1(b) and 1(c).

Temperature-dependent resistivity for pressures up to 2.86 and 7.5 GPa are shown in Figs. 1(b) and 1(c), respectively. At ambient pressure, the jump in the resistivity at T_{MI} is very sharp. For resistivity measurements at 0.84 and 1.64 GPa, the higher temperature ($T > T_{MI}$) resistivity decreases with increasing temperature. This was likely caused by the electrical connection between the sample and the cell, mentioned above. Subsequent measurements with other cells without such electrical connections had more metal-like $\rho(T)$ behavior with the high-temperature resistivity increasing with increasing temperature consistent with the behavior seen at ambient pressure. For $0 < P < 3.92$ GPa, the MI transition temperature was taken as the intersection of the extrapolated lines seen in Fig. 1(c) on the $P = 2.86$ GPa resistivity curve.

For V_6O_{11}, the 1:1 FC70 : FC770 mixture was used as the liquid pressure medium. Near 10 K at ambient pressure, the resistivity in the insulating state reaches a maximum and decreases with further lowering of temperature. As pressure is applied, T_{MI} is gradually suppressed and the insulating state maxima are reduced in magnitude and shifted to higher temperatures. By 3.52 GPa, there is only a small discontinuous jump in the resistivity near 46 K, which is likely a remnant signature of the MI transition. The upper inset of Fig. 1(c) shows both the cooling and warming data for this pressure confirming the presence of the hysteresis at pressures close to P_c^{MI}. The width of the hysteresis is ~6 K, which is considerably larger than the temperature lag from cooling and warming of the cell. At the next higher pressure (3.92 GPa), where the MI transition has disappeared, there is virtually no hysteresis between the cooling and warming data. Above P_c^{MI}, the resistivity shows no MI transition and instead declines smoothly and faster at low temperatures revealing T^2 dependence near base temperatures.

Resistivity measurements just above P_c^{MI} were done under a pressure of 3.87 GPa down to 0.47 K [lower inset of Fig. 1(c)]. There were no indications of any low-temperature phase transitions (e.g., superconductivity) and instead FL behavior was seen up to 2.1 K. Further pressure increases up to 7.52 GPa

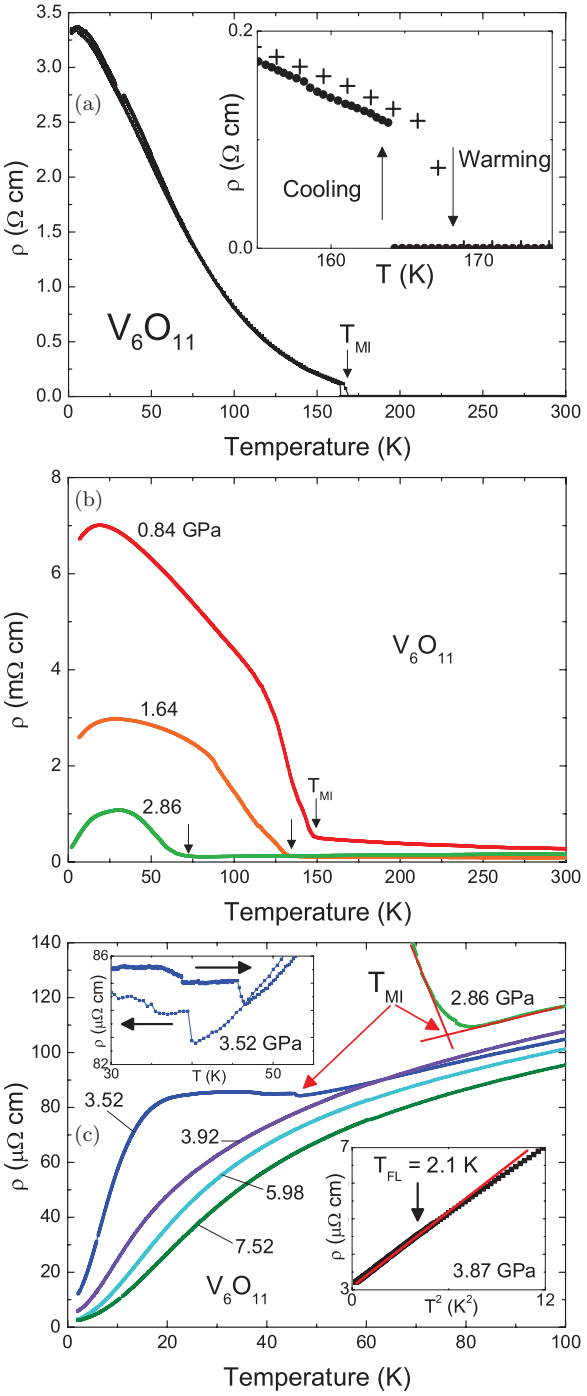

FIG. 1. (Color online) Resistivity curves for V_6O_{11} under pressure. For clarity, not all data sets are shown. (a) Ambient pressure resistivity for cooling and warming data. The arrow indicates the MI transition temperature. The inset shows the hysteresis of the MI transition near 170 K. (b) Resistivity measurements at $P = 0.84$, 1.64, and 2.86 GPa show suppression of T_{MI} (indicated by the arrows) with applied pressure. (c) Resistivity measurements for $P = 2.86$, 3.52, 3.92, 5.98, and 7.52 GPa are shown on a $\mu\Omega$ cm scale. The criterion used for determining the MI transition is illustrated on the $P = 2.86$ GPa curve. The upper inset shows the hysteresis of the MI transition at 3.52 GPa with arrows indicating the cooling and warming data. The lower inset shows resistivity versus T^2 data down to 0.47 K at 3.87 GPa and a fit to the low-temperature data. The arrow indicates the onset of low-temperature Fermi-liquid-like, $\rho \propto T^2$, behavior.

caused a systematic reduction of the resistivity across the measured temperature range and an increase of the temperature region of FL behavior to 6.8 K.

B. V_7O_{13}

Resistivity curves for V_7O_{13} at various pressures are shown in Fig. 2 where 1:1 FC70 : FC770 was used as the liquid pressure medium. At ambient pressure, the resistivity remains metallic down to 2 K. At ~43.5 K, there is a clear resistive anomaly, as was seen in previous studies[10,11,13,15] and had been associated with the AFM transition seen in the susceptibility data.[10,11,13] The AFM transition temperature, T_N, was inferred from the minimum of the derivative of the resistivity [inset of Fig. 2(a)]. Upon lowering the temperature below T_N, there is a rapid decrease of resistivity with T^2 behavior emerging at low temperatures. As pressure is increased, the resistive anomaly shifts to lower temperatures, and disappears between 2.99 and 4.0 GPa. Pressure increases beyond P_c^{AFM} expand the T^2 region and the coefficient of T^2 resistivity, A, decreases rapidly.

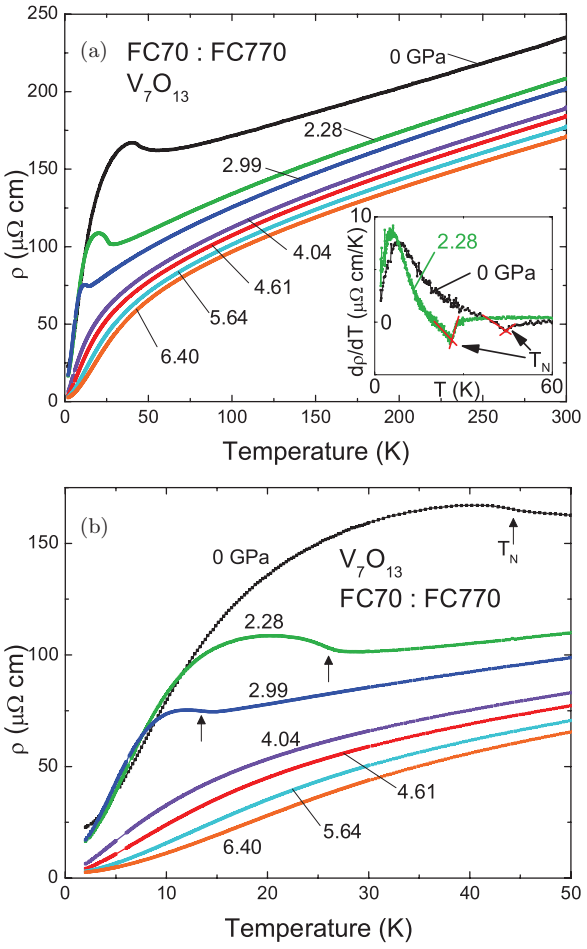

FIG. 2. (Color online) Resistivity measurements under pressure for V_7O_{13} where the 1:1 FC70 : FC770 mix was used as the pressure medium. Only a few selected resistivity curves are shown for clarity. (a) Full temperature range of measurements show metallic behavior of V_7O_{13}. Inset shows $d\rho/dT$ and the criterion used for determining the AFM transition temperature. (b) Low-temperature resistivity data with arrows indicating the AFM transition temperature.

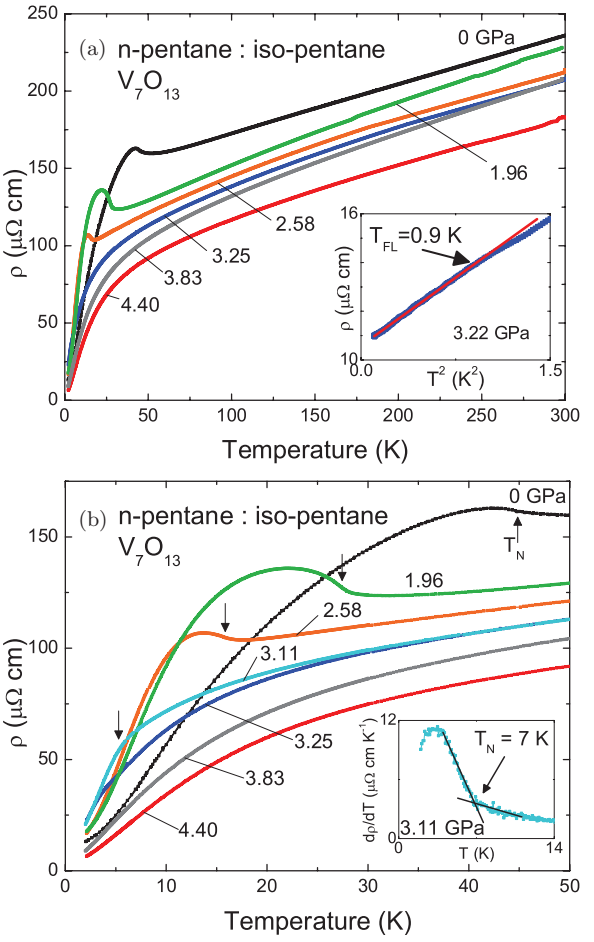

FIG. 3. (Color online) Resistivity measurements under pressure using the more hydrostatic 1:1 n-pentane : iso-pentane mixture as the pressure medium. (a) The full temperature range is shown with selected curves from two different sets of measurements. Inset shows the low-temperature T^2 fit for 3.22 GPa measured down to 0.32 K. (b) The low-temperature resistivity data is shown, with the kinklike feature in the 3.11 and 3.25 GPa measurements that is likely a remnant signature of AFM ordering. The arrows the AFM transition temperature. The inset shows $d\rho/dT$ for $P = 3.11$ GPa that where the feature is more noticeable and T_N determined.

For measurements with improved hydrostaticity, a 1:1 n-pentane : iso-pentane mix was used for several pressure measurements. Results are shown in Fig. 3. Pressures closer to P_c^{AFM} were reached [3.11, 3.25, and 3.83 GPa are shown in Fig. 3(b)] and the low-temperature resistivity data for $P = 3.11$ and 3.25 GPa show a noticeable change in slope. This feature is better seen in the temperature derivative of the resistivity [inset of Fig. 3(b)] and appears to be related to the feature that has been associated with AFM order, which is suppressed at a higher pressure. Above 3.25 GPa, the resistivity curves remain smooth down to base temperature with a widening range of T^2 behavior (as pressure increases) at low temperatures. The critical pressure is inferred to be between 3.25 and 3.83 GPa.

Measurements of V_7O_{13} at 3.22 and 3.83 GPa down to 0.32 K showed no indications of any low-temperature phase transitions. An example of a fit to T^2 behavior is shown in the inset of Fig. 3(a) for 3.22 GPa.

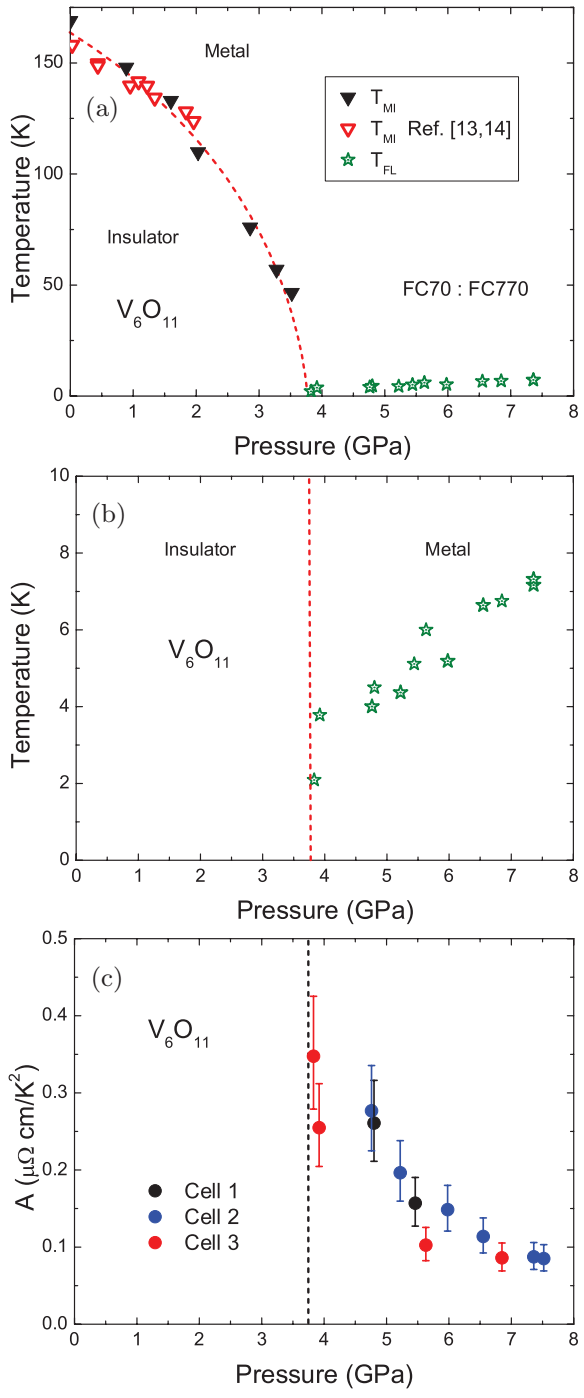

FIG. 4. (Color online) (a) Phase diagram of V_6O_{11} illustrating the salient features as they progress with pressure. Triangles denote the MI transition temperature (T_{MI}) and the open stars with a central dot denote the upper limit of FL behavior (T_{FL}). The open red triangles are data from a study by Canfield *et al*. (Refs. 13 and 14). The red dashed line is a guide to the eye. (b) The range of the Fermi-liquid behavior, that the V_6O_{11} $\rho(T)$ data can be fit when it is metallic throughout the full temperature range. (c) T^2 coefficient of the resistivity versus pressure phase diagram. The black dashed vertical line indicates the first pressure where the MI transition has been fully suppressed.

IV. ANALYSIS AND DISCUSSION

Figure 4(a) presents temperature-pressure data that form a phase diagram of the MI transition for V_6O_{11} and the progression of the range of low temperature, $\rho \propto T^2$, FL behavior. The T_{MI} data overlap those from a previous study by Canfield *et al*. where measurements up to 1.87 GPa showed a linear decrease in T_{MI} with pressure,[14] but, as shown in Fig. 4(a), the new data show a somewhat larger dT_{MI}/dP value and clear, nonlinear suppression of T_{MI} with pressure until T_{MI} disappears between 3.52 and 3.87 GPa. The suppression of T_{MI} indicates the occurrence of a quantum phase transition driven by a nonthermal parameter, in this case, pressure. At 3.87 GPa, just above P_c^{MI}, the low-temperature resistivity measurements down to 0.47 K showed $\rho \propto T^2$ behavior for $T < 2.1$ K [inset of Fig. 1(c)]. As pressure increases beyond P_c^{MI}, T_{FL} increases monotonically [Fig. 4(b)] and the coefficient A decreases [Fig. 4(c)]. The pressure dependence of both T_{FL} and A are not consistent with divergent behavior at P_c^{MI} but rather seem to manifest a low-pressure truncation below P_c^{MI}. This is not too surprising given that the transition being suppressed maintains its first-order nature [as evidenced by the hysteretic behavior of the MI transition close to P_c^{MI} shown in the upper inset of Fig. 1(c)] down to the lowest detectable values of T_{MI}. Therefore, the divergence of A associated with T_{FL} going to zero at a quantum critical point is not seen in V_6O_{11}.

For V_7O_{13}, the suppression of the second-order AFM transition temperature with pressure can be seen in Fig. 5(a), with data from past studies using different liquid media included for comparison. The data match well for the liquid media with lower hydrostatic limits, namely 1:1 FC70 : FC770 and the Daphne 7373 mixtures with hydrostatic limits of 1 and 2.2 GPa respectively.[23,27] The evolution of T_N with pressure shows a small dependence on the choice of pressure medium. This is not unexpected, as it has been seen before that the choice of pressure medium can affect the pressure dependence of a magnetic transition temperature.[26] For the measurements with the 1:1 n-pentane : iso-pentane media, with a higher hydrostatic limit of 6.5 GPa,[24] the AFM transition temperatures tend to be lower at a given pressure. In our measurements, despite the minute difference in T_N suppression rates due to the choice of liquid medium, an extrapolation of T_N shows that the critical pressure of $P_c^{AFM} = 3.5$ GPa is very nearly the same and may at most, differ by 0.2 GPa for different liquid media. $\rho \propto T^2$ fits to the low-temperature resistivity data for V_7O_{13} were used to infer T_{FL} as shown in the phase diagrams Figs. 5(a) and 5(b).

There is a large region of Fermi-liquid behavior at ambient pressure, up to 8.6 K, and this region diminishes as pressure is increased to P_c^{AFM}. For two pressures close to P_c^{AFM}, 3.22 and 3.83 GPa, measurements down to 0.32 K revealed quadratic behavior at very low temperatures. For 3.22 GPa, this quadratic behavior persisted up to 0.9 K with the highest T^2 coefficient found, $A = 3.7 \times 10^{-6}\ \Omega\,\mathrm{cm\,K^{-2}}$. For 3.83 GPa, the quadratic behavior is seen up to 1.2 K ($T^2 = 1.4$ K). Above P_c^{AFM} for V_7O_{13}, the T^2 coefficient decreases (roughly inversely with $P - P_c^{AFM}$) and the temperature region of Fermi-liquid behavior increases rapidly to nearly 4 K. The contributions to the scattering due to the magnetic excitations (below T_N) and fluctuations (above T_N) may have different prefactors, but the data clearly shows T^2 resistivity at low temperatures on both sides of P_c^{AFM}.

A hallmark feature of a QCP is the divergent behavior of the T^2 coefficient near the critical point. The divergence has been fit to $A \propto |P - P_c^{AFM}|^{-1}$ on either side of $P_c^{AFM} = 3.5$ GPa in

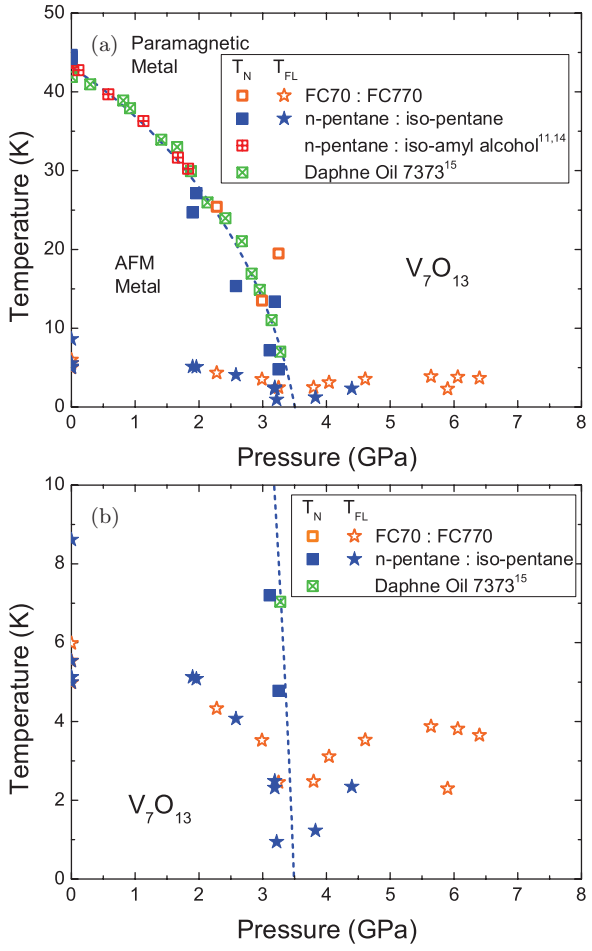

FIG. 5. (Color online) Phase diagrams for V_7O_{13}. (a) T_N as it is suppressed by pressure. The blue dashed line is a guide for the eye. (b) Expanded, low-temperature region showing T_{FL} (range of Fermi-liquid behavior), the blue dashed line shows the extrapolation of the $T_N(P)$ line.

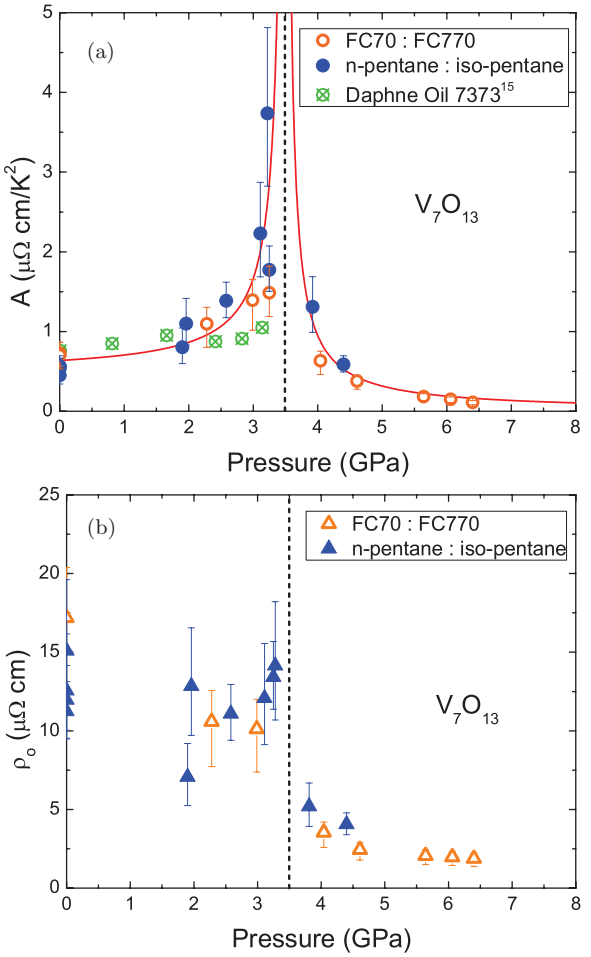

FIG. 6. (Color online) Phase diagrams for V_7O_{13}. (a) T^2 coefficient as it evolves with pressure. The red lines are fits of the results from measurements with the 1:1 n-pentane : iso-pentane and 1:1 FC70 : FC770 mixtures with the form of $A \propto |P - P_c^{\mathrm{AFM}}|^{-1}$ where $P_c^{\mathrm{AFM}} = 3.5$ GPa is denoted as the dashed vertical black line. Open and closed symbols are for measurements with 1:1 FC70 : FC770 and 1:1 n-pentane : iso-pentane media, respectively. For comparison, results from previous studies (Refs. 11,14 and 15) are also plotted and can be seen as the crossed symbols. (b) ρ_0 inferred from T^2 fits.

Fig. 6(a) (shown as the solid red line). Another indication of a QCP is a sharp drop of ρ_0 at the critical pressure. A phase diagram of ρ_0 vs pressure is shown in Fig. 6(b) showing a modest rise as pressure is increased up to P_c^{AFM} and a sharp drop at pressures just above.

A past study[15] down to $T = 1.7$ K showed a $T^{3/2}$ dependence at $P_c^{\mathrm{AFM}} = 3.4$ GPa at base temperatures, consistent with self-consistent renormalization theory for spin fluctuations near a QCP for a three-dimensional (3D) AFM.[28] Unfortunately, in our body of work, measurements closer to 3.4 GPa were not taken due to the difficulty of controlling the increase of pressure by anything less than 0.5 GPa. Measurements with the PPMS at 3.28 GPa do show a $T^{3/2}$ dependence from 2 to 2.3 K. However, upon closer inspection of lower temperature measurements down to 0.32 K at $P_c^{\mathrm{AFM}} = 3.22$ GPa, the resistivity shows T^2 dependence up to 0.9 K (Fig. 7). This behavior is not unexpected near a QCP where the Fermi-liquid behavior has been significantly suppressed. The fact that FL behavior only exists at low temperatures indicates that at 3.22 GPa, we are close to the quantum critical point.

Measuring with a more hydrostatic medium (the 1:1 n-pentane : iso-pentane mix), shows that the divergence of A at

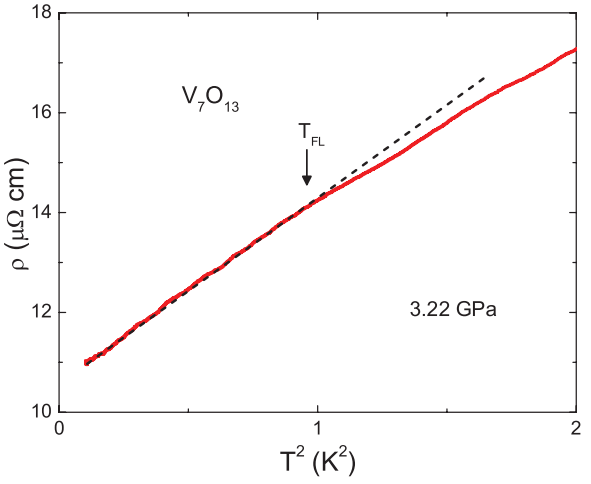

FIG. 7. (Color online) Resistivity plotted versus T^2 showing the low-temperature FL behavior up to ~1 K.

P_c^{AFM} is stronger than was seen when using the less hydrostatic 1:1 FC70 : FC770 mix. This might be the cause of the reduced divergent behavior of A near P_c^{AFM} seen in previous measurements of V_7O_{13}[15] where Daphne Oil 7373 was used as the liquid pressure medium. With a room temperature solidification pressure of 2.2 GPa,[27] Daphne Oil 7373 has better hydrostaticity than the 1:1 FC70 : FC770 mixture, which solidifies near 1 GPa but is still less hydrostatic than the 1:1 n-pentane : iso-pentane mixture which has a solidification pressure of 6.5 GPa.[23,24] Improved hydrostaticity decreases the pressure gradients across the sample and improves its homogeneity, which is essential when studying the narrow pressure region where quantum fluctuations can drive a magnetic quantum phase transition.

A composite phase diagram for V_6O_{11}, V_7O_{13}, and V_8O_{15}, is shown in Fig. 8(a) with data from past pressure measurements included for comparison.[11,14] The pressure dependence of T_N for V_7O_{13} is remarkably consistent for measurements using different liquid media. Even more surprising is a comparison of $T_N(P)$ for V_7O_{13} to V_8O_{15}. For V_8O_{15}, pressure suppresses the MI transition fast enough to reveal the low-temperature AFM transition in the resistivity. The pressure dependence of this AFM transition for V_8O_{15} directly maps onto the same for V_7O_{13} without any shifts in pressure or normalizations to T_N. $T_N(P)$ is virtually identical for V_7O_{13} and V_8O_{15}, giving rise to the possibility that it is a universal feature of the low-temperature metallic state of the Magnéli series.

The composite phase diagram shown in Fig. 8(a) helps explain several of the features that emerge in the V_6O_{11} data set. First of all, the fact that signatures of an antiferromagnetic phase transition, similar to those seen for V_7O_{13} and V_8O_{15}, are missing in V_6O_{11} at any measured pressure can be understood by noting that the $T_N(P)$ line goes to zero before the critical pressure for the complete suppression of the MI transition in V_6O_{11}. This means that, for V_6O_{11}, we cannot directly access a QCP associated with antiferromagnetic order. This being said, though, Fig. 8(a) does show that, as the pressure applied to V_6O_{11} is decreased from the high-pressure side (i.e., as we progress from 7 GPa toward 4 GPa) the sample, at low temperatures is approaching not only the quantum phase transition associated with the end point of the $T_{MI}(P)$ line, but also may be approaching a hidden QCP associated with the potential antiferromagnetic ordering seen for V_7O_{13} and V_8O_{15}. This possibility is explored more fully in Figs. 8(b) and 8(c) where the pressure dependencies of T_{FL} and A as a function of P are plotted for both V_7O_{13} and V_6O_{11}. For V_6O_{11}, the evolution of T_{FL} with pressure is consistent with the possibility that the FL behavior is associated with the antiferromagnetic fluctuations that gradually weaken with the increase of pressure. The $A(P)$ data is similar for $P > 5$ GPa, but for $3.8 < P < 5$ GPa the A values for V_6O_{11} are significantly smaller than those for V_7O_{13}. This may, of course, be due to the fact that whereas for V_7O_{13} we can experimentally pass through the critical pressure for the QCP, we cannot approach the QCP so closely for V_6O_{11} given the higher pressure $T_{MI}(P)$ line.

Consequently, it is of interest to do further studies on a member of this Magnéli series with a lower MI transition at ambient pressure. V_9O_{17}, which has a MI transition at

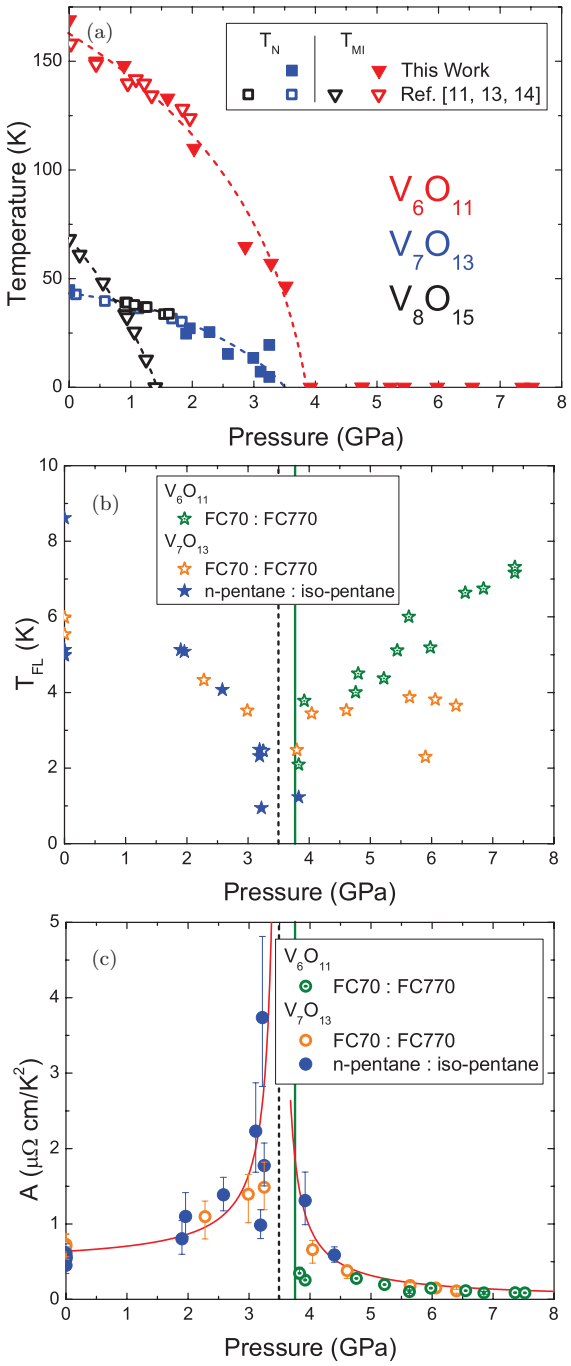

FIG. 8. (Color online) (a) Composite phase diagram of V_6O_{11}, V_7O_{13}, and V_8O_{15} with the latter data from work by Canfield *et al.* (Refs. 11,13 and 14). The AFM transition of V_7O_{13} and V_8O_{15} overlap, however, the MI transition of V_6O_{11} persists near the AFM critical pressure, negating any possibility of seeing a splitting of the MI and AFM transition as in V_8O_{15}. The dashed lines are guides for the eye. (b) Combined phase diagram of T_{FL} for V_6O_{11} (shown as green open stars with a central dot) and V_7O_{13} (shown as orange open and blue closed stars). The solid red line is a fit to the V_7O_{13} data as described before. (c) Combined phase diagram of T^2 coefficient for V_6O_{11} (shown as green circles with a central dot) and V_7O_{13} (shown as orange open and blue closed circles indicating the use of 1:1 FC70 : FC770 and 1:1 n-pentane : iso-pentane liquid media, respectively). The black dashed line indicates P_c^{AFM} for V_7O_{13} and the green solid line indicates P_c^{MI} for V_6O_{11}.

79 K would be a natural choice as its T_{MI} is slightly higher than that of V_8O_{15}.[9] Another possible candidate for pressure measurements is V_5O_9 with $T_{MI}\sim 130$ K.[4,8,14,29] Previous studies of V_5O_9 with pressure measurements up to 0.85 and 1.73 GPa show a linear suppression of T_{MI} at a rate of about 9 K/GPa.[14,30] Such a low suppression rate would consign it to the same fate as V_6O_{11} where the MI transition is too robust for the region $P < 3.5$ GPa. However, if this rate increases with pressure, as it did for V_6O_{11} and V_8O_{15}, then combined with its somewhat low T_{MI}, it may be possible to suppress T_{MI} sufficiently to see the AFM feature emerge in the low-temperature metallic state, or possibly even revealing a different ground state.

V. CONCLUSION

The electrical transport properties of V_6O_{11} and V_7O_{13} have been measured under pressures up to 7.52 and 6.40 GPa, respectively. The MI transition in V_6O_{11} was fully suppressed by 3.87 GPa which overshoots the AFM critical pressure for V_7O_{13} where $P_c^{AFM} = 3.5$ GPa. The suppression of the AFM temperature in V_7O_{13} with pressure maps directly to the same seen in V_8O_{15} suggesting that this is a universal characteristic of the members of this Magnéli series. However, the robust MI transition in V_6O_{11} is not fully suppressed until after the AFM critical pressure in V_7O_{13}. Therefore, no AFM ordering was seen for V_6O_{11}.

Resistivity measurements under pressure for V_7O_{13} show that the AFM transition temperature is gradually suppressed with pressure until it is gone by 3.83 GPa. The divergent behavior of the T^2 coefficient with $P_c^{AFM} = 3.5$ GPa indicates proximity to a quantum critical point. A previously reported region of $T^{3/2}$ behavior was found to be in fact a crossover region to FL behavior at even lower temperatures below 0.9 K.

Although the P-T phase diagram for V_6O_{11} does not show any long-range magnetic order (of the kind found in V_7O_{13}), there is clear Fermi-liquid behavior at low temperatures, above P_c^{MI} with the T_{FL} value diminishing as P_c^{MI} was approached from higher pressures. These data suggest that there might well be a hidden QCP in V_6O_{11} that can only be inferred from the extrapolation of high-pressure T_{FL} results.

ACKNOWLEDGMENTS

The authors would like to thank H. Hodovanets, V. Taufour, E. D. Mun, and M. Torikachvili for many fruitful discussions as well as expert technical assistance. This work was carried out at Ames Laboratory, US DOE, under Contract No. DE-AC02-07CH11358. S.L.B. acknowledges partial support from the State of Iowa through Iowa State University.

*Present address: Alstom Grid, 69100 Villeurbanne, France.
†Present address: Los Alamos National Laboratory, Los Alamos, New Mexico 87544, USA.

[1] N. Mott, *Metal-Insulator Transitions: Second Edition* (Taylor and Francis, London, 1990).
[2] D. B. McWhan and T. M. Rice, Phys. Rev. Lett. **22**, 887 (1969).
[3] C. N. Berglund and H. J. Guggenheim, Phys. Rev. **185**, 1022 (1969).
[4] S. Kachi, K. Kosuge, and H. Okinaka, J. Solid State Chem. **6**, 258 (1973).
[5] C. N. Berglund and A. Jayaraman, Phys. Rev. **185**, 1034 (1969).
[6] K. Kosuge, H. Okinaka, and S. Kachi, IEEE T. Magn. **8**, 581 (1972).
[7] A. C. Gossard, F. J. Di Salvo, L. C. Erich, J. P. Remeika, H. Yasuoka, K. Kosuge, and S. Kachi, Phys. Rev. B **10**, 4178 (1974).
[8] S. Nagata, B. F. Griffing, G. D. Khattak, and P. H. Keesom, J. Appl. Phys. **50**, 7575 (1979).
[9] H. Kuwamoto, N. Otsuka, and H. Sato, J. Solid State Chem. **36**, 133 (1981).
[10] B. F. Griffing, S. A. Shivashankar, S. Nagata, S. P. Faile, and J. M. Honig, Phys. Rev. B **25**, 1703 (1982).
[11] P. C. Canfield, J. D. Thompson, and G. Gruner, Phys. Rev. B **41**, 4850 (1990).
[12] S. Åsbrink and M. Malinowski, J. Appl. Crystallogr. **20**, 195 (1987).
[13] P. Canfield, J. Thompson, and G. Grüner, Physica B **163**, 191 (1990).
[14] P. C. Canfield, Ph.D. thesis, University of California, Los Angeles, 1990.
[15] H. Ueda, K. Kitazawa, T. Matsumoto, and H. Takagi, Solid State Commun. **125**, 83 (2003).
[16] V. Sidorov, A. Waśkowska, and D. Badurski, Solid State Commun. **125**, 359 (2003).
[17] A. Perucchi, L. Baldassarre, E. Arcangeletti, D. D. Castro, P. Postorino, and S. Lupi, Infrared Phys. Technol. **51**, 440 (2008).
[18] K. Nagasawa, Y. Bando, and T. Takada, Jpn. J. Appl. Phys. **8**, 1267 (1969).
[19] H. Okinaka, K. Nagasawa, K. Kosuge, Y. Bando, S. Kachi, and T. Takada, J. Phys. Soc. Jpn. **29**, 245 (1970).
[20] H. V. Keer, R. D. Swarnakar, and S. P. Faile, J. Phys. C **10**, L637 (1977).
[21] E. Colombier and D. Braithwaite, Rev. Sci. Instrum. **78**, 093903 (2007).
[22] T. Varga, A. P. Wilkinson, and R. J. Angel, Rev. Sci. Instrum. **74**, 4564 (2003).
[23] V. A. Sidorov and R. A. Sadykov, J. Phys.: Condens. Matter **17**, S3005 (2005).
[24] S. K. Kim, M. S. Torikachvili, E. Colombier, A. Thaler, S. L. Bud'ko, and P. C. Canfield, Phys. Rev. B **84**, 134525 (2011).
[25] E. Colombier, M. S. Torikachvili, N. Ni, A. Thaler, S. L. Bud'ko, and P. C. Canfield, Supercond. Sci. Technol. **23**, 054003 (2010).
[26] E. Colombier, G. Knebel, B. Salce, E. D. Mun, X. Lin, S. L. Bud'ko, and P. C. Canfield, Phys. Rev. B **84**, 064442 (2011).
[27] K. Yokogawa, K. Murata, H. Yoshino, and S. Aoyama, Jpn. J. Appl. Phys. **46**, 3636 (2007).
[28] T. Moriya and K. Ueda, Rep. Prog. Phys. **66**, 1299 (2003).
[29] A. D. Inglis, C. M. Hurd, and P. Strobel, J. Phys. C **17**, 6801 (1984).
[30] E. I. Terukov, Y. Z. Sanfirov, and A. Y. Zyuzin, Fiz. Tverd. Tela **21**, 1563 (1979).